Remote Sensing of Environment 140 (2014) 94–106

Contents lists available at ScienceDirect

Remote Sensing of Environment

journal homepage: www.elsevier.com/locate/rse

Land subsidence in central Mexico detected by ALOS InSAR time-series

Estelle Chaussard [a,*], Shimon Wdowinski [a], Enrique Cabral-Cano [b], Falk Amelung [a]

[a] School of Marine and Atmospheric Science, University of Miami, Miami, FL 33149-1098, USA
[b] Departamento de Geomagnetismo y Expiración, Instituto de Geofísica, Universidad Nacional, Autónoma de México, Ciudad Universitaria, México D.F., 04510, Mexico

ARTICLE INFO

Article history:
Received 19 May 2013
Received in revised form 23 August 2013
Accepted 24 August 2013
Available online xxxx

Keywords:
Land subsidence
InSAR
SBAS time-series
Mexico
Tectonics
Groundwater
Faults

ABSTRACT

Massive groundwater extraction is common throughout Mexico and is well known to result in land subsidence. However, most land subsidence surveys focus on one single city, mainly Mexico City, and thus fail to reveal the regional extent of the problem. Here we use 2007–2011 Interferometric Synthetic Aperture Radar (InSAR) time-series analysis of ALOS data to resolve land subsidence in the entire central Mexico region. We identify land subsidence in 21 areas, including 17 cities. Linear vertical rates over 30 cm/yr are observed in Mexico City, while in the other locations rates of 5–10 cm/yr are detected. We define 3 main categories of subsidence using the averaged velocity maps in conjunction with previously published structural, surface geology, and land use mapping: (1) rapid, large-scale subsidence, (2) rapid, local-scale subsidence, and (3) slow, patchy subsidence. The correlation between subsidence and land use confirms that groundwater extraction mainly for agricultural and urban activities is the main cause of land subsidence. We observe that the boundaries of the subsiding areas are typically characterized by high velocity gradients often coinciding with pre-existing faults, motion on these faults being driven by water extraction rather than by tectonic activity. Regional surveys of this type are necessary to understand the spatial and temporal evolution of land subsidence, to constrain the distribution and connectivity of water-bearing units, and ultimately to reach better hazard mitigation plans.

1. Introduction

In Mexico groundwater extraction from local aquifers is the primary source of water supply and contributes to more than 70% of the water needs of the 112 million inhabitants (INEGI, 2011). Overexploitation of the groundwater resources has led to consolidation of the aquifer systems (aquifers and aquitards), resulting in rapid land subsidence associated with colossal societal impacts. Areas affected by rapid differential subsidence suffer from damages to infrastructures, especially significant in Mexico where many colonial-era cities are included in the UNESCO World Heritage list (e.g. Carreón-Freyre, Cerca, & Hernández Marín, 2005; Julio-Miranda, Ortíz-Rodríguez, Palacio-Aponte, López-Doncel, & Barboza-Gudiño, 2012; Osmanoglu, Dixon, Wdowinski, Cabral-Cano, & Jiang, 2011; Pacheco et al., 2006). Indirect consequences also include a decrease in water resources and an increase in flood risk and water contamination, all endangering human lives and resulting in heavy financial burdens for local government administrations (e.g. Cabral-Cano et al., 2008; Ortiz-Zamora & Ortega-Guerrero, 2010).

Mapping of land subsidence with high precision can be achieved using the differential InSAR technique (D-InSAR) (e.g. Strozzi & Wegmuller, 1999) which measures ground displacement in the radar line-of-sight (LOS) direction of a satellite (or airplane) by computing the phase difference of 2 temporally separated SAR images (Gabriel, Goldstein, & Zebker, 1989; Massonnet et al., 1993). Time dependent subsidence monitoring traditionally relies on time-series techniques such as persistent scatterer interferometry (PSI) (e.g. Bock, Wdowinski, Ferretti, Novali, & Fumagalli, 2012; Kampes, 2005, 2006; Osmanoglu et al., 2011), small baseline (SB) interferometry (e.g. Berardino, Fornaro, Lanari, & Sansosti, 2002; Casu, Manzo, & Lanari, 2006; Lanari et al., 2007; Usai, 2003), and joint analysis of these two (e.g.; Ferretti et al., 2011; Yan et al., 2012). Each technique is best matched to a particular set of conditions: PSI enables precise characterization of linear deformation affecting "persistent scatterers" abundant in urban areas (Bell, Amelung, Ferretti, Bianchi, & Novali, 2008; Bürgmann et al., 2006; Colesanti, Ferretti, Novali, Prati, & Rocca, 2003), SB reduces decorrelation in areas with high deformation rates (Gourmelen, Amelung, Casu, Manzo, & Lanari, 2007; Gourmelen, Amelung, & Lanari, 2010; Hooper, 2006), and joint methods enable retrieving large phase changes of "distributed scaterrers" relying on complex processing. To characterize rapid subsidence on a large scale in both urban and agricultural settings the SB technique relying on L-Band SAR data is best suited.

While many Mexican cities are developed on lacustrine and intramontane basins filled with compressible deposits and thus prone to land subsidence, only a few medium to large-sized cities are known to subside (Cabral-Cano et al., 2008; Cigna, Cabral-Cano, Osmanoglu, Dixon, & Wdowinski, 2011, Cigna et al., 2012; Farina, Avila-Olivera, & Garduño-Monroy, 2007; Huizar-Álvarez, Mitre-Salazar, Marín-Córdova, Trujillo-Candelaria, & Martínez-Reyes, 2011). This disparity is likely due to the fact that both geotechnical studies and detailed subsidence mapping efforts focus on one single city, and often on Mexico City, known to

* Corresponding author at: Department of Earth and Planetary Science, University of California, Berkeley, Berkeley, CA 94720-4767, USA.

0034-4257/$ – see front matter © 2013 Elsevier Inc. All rights reserved.
http://dx.doi.org/10.1016/j.rse.2013.08.038

subside since the 1920s (e.g. Gayol, 1925; Hiriart & Marsal, 1969; López-Quiroz, Doin, Tupin, Briole, & Nicolas, 2009; Osmanoglu et al., 2011; Yan et al., 2012). Thus, there is a lack of knowledge of the spatial extension, magnitude, and temporal evolution of land subsidence elsewhere in Mexico.

To fill this gap we conduct an InSAR-SB time-series survey covering the entire central Mexico area. Such regional observations are useful for the development of hazard mitigation plans and to reach a more efficient use of ground-based monitoring networks. Moreover, because InSAR time-series allow detailed mapping of land subsidence we evaluate relations between subsidence, faults, surface geology, and type of land use to better understand the parameters causing and influencing the distribution and temporal evolution of land subsidence.

This paper is organized as follows. We first discuss the potential for land subsidence in Mexico and justify the location of our survey area (Section 2). After summarizing the data and methods used (Section 3), we introduce the InSAR-measured subsidence organized by categories (Section 4). We then compare our results with previous studies and discuss the causes of subsidence, address the roles played by the surface geology and pre-existing faults, and the lack of seasonal variability (Section 5).

2. Potential for land subsidence in Mexico

Overexploitation of groundwater and associated decrease in pore-water pressure has led to compression of the granular skeleton of the aquifers (sand and gravel deposits) and aquitards (silt and clay), and to wide spread consolidation of these compressible deposits in Mexico (Leake, 1990). The deformation in an aquifer system is purely elastic (recoverable) when the maximum historical stress is not exceeded (Poland, 1961); in the opposite case sediments, and mostly aquitards, undergo irreversible rearrangement of their pore structures (Terzaghi, 1925). Areas with thicker compressible deposits experience faster and more widespread land subsidence (Helm, 1978). Thus, highly populated areas, where groundwater extraction likely occurs, located on compressible deposits have a high subsidence potential.

The population density of Mexico and the distribution of compressible deposits are shown in Fig. 1. Most of the areas with over 250 persons per km^2 (dark orange colors) are located in an east–west oriented belt in central Mexico surrounding the Transmexican Volcanic Belt (TMVB). Compressible deposits occur along the coasts and in two other areas. First, in the same east–west oriented belt of central Mexico where high population density is observed. There, volcanic structures and normal faults due to the extensive stress regime result in the formation of basins and grabens favorable to the accumulation of compressible deposits (García-Palomo, Macías, & Garduno, 2000; Singh & Pardo, 1993). Second, in a north–south oriented region in the central part of Mexico, between the Sierra Madre Oriental and Occidental where normal faults due to the Cenozoic extensive stresses favored the formation of grabens (Alaniz-Álvarez & Nieto-Samaniego, 2007 and references therein). The remaining parts of Mexico are constituted of relatively incompressible deposits, volcanic and metamorphic rocks, less likely to experience subsidence (Servicio Geologico Mexicano, 1998).

We conduct a survey of the east–west belt of central Mexico, characterized by high population density and compressible deposits (red rectangle in Fig. 1, cities with >100, 000 people are shown in the inset). This region includes cities with known subsidence such as Mexico City, Morelia, Aguascalientes, and Celaya (Cabral-Cano et al., 2008; Cigna et al., 2011, 2012; Huizar-Álvarez et al., 2011).

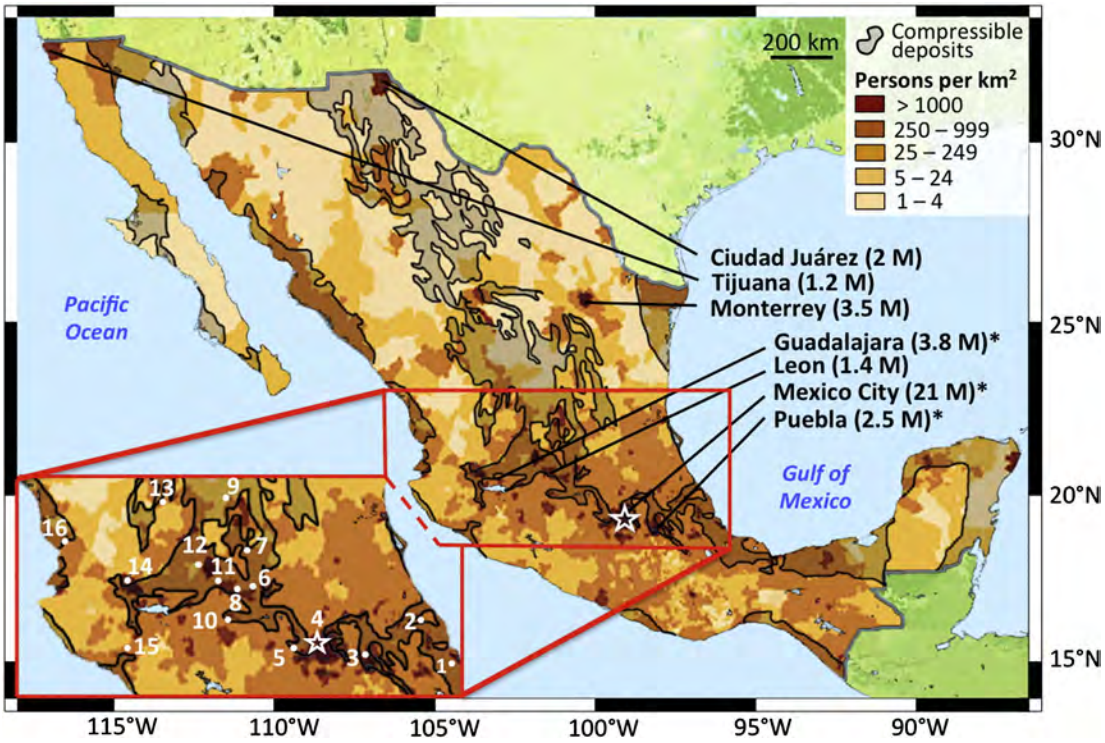

Fig. 1. Map of the population density in Mexico from the Gridded Population of the World, Version 3 (GPWv3) based on the 2000 census (Center for International Earth Science Information Network (CIESIN), Columbia University, & Centro Internacional de Agricultura Tropical (CIAT) (CIAT), 2005). Cities with over 1 million inhabitants are shown with their respective population and cities included in the UNESCO World Heritage list are marked with an asterisk. A star marks the capital, Mexico City. Most of the highly populated areas (dark orange to brown colors) are located in central Mexico. The distribution of compressible deposits is shown by black contours and dark overlays (Servicio Geologico Mexicano, 1998). The red rectangle marks our survey area in central Mexico where highly populated areas are developed in compressible deposits. A zoom in this area is shown in the bottom left inset and cities with over 100,000 inhabitants are marked by white dots and numbered. The cities are numbered from east to west and correspond to 1 = Veracruz, 2 = Xalapa, 3 = Puebla, 4 = Mexico City, 5 = Toluca, 6 = Queretaro*, 7 = San Luis de la Paz, 8 = Celaya, 9 = San Luis Potosí, 10 = Morelia*, 11 = Irapuato, 12 = Leon, 13 = Aguascalientes, 14 = Guadalajara, 15 = Colima, and 16 = Tepic. (For interpretation of the references to color in this figure legend, the reader is referred to the web version of this article.)

3. Data coverage and method

We use over 600 SAR images from 15 ascending tracks acquired by the ALOS satellite between 2007 and 2011, to survey an area of 200,000 km^2 in central Mexico. We cover 4 of the 7 Mexican cities with over 1 million inhabitants (comprised in the red rectangle in Fig. 1) and 12 other cities with a population of over 100, 000 (Veracruz, Xalapa, Toluca, Queretaro, San Luis de la Paz, San Luis Potosí, Morelia, Celaya, Irapuato, Aguascalientes, Colima, and Tepic, from east to west in Fig. 1). For our 4 yr period we have an average of 13 acquisitions per frame (Table 1).

InSAR measures ground displacement in the radar line-of-sight (LOS) direction that occurred between two SAR acquisitions. We use the ROI_PAC processing software developed at NASA's Jet Propulsion Laboratory (JPL) (Rosen, Hensley, Peltzer, & Simons, 2004) to produce over 3000 interferograms, and the small baseline (SB) method for generating the InSAR time-series (Berardino et al., 2002; Gourmelen et al., 2010; Lanari et al., 2004). The SB method relies on the redundancy of multiple SAR images to determine the surface displacement through time. Only interferograms with small spatial (<1.5 km) and temporal (<1 yr) baselines are used to maintain high coherence and create an interconnected network of interferograms (e.g. Chaussard, Amelung, & Aoki, 2013). The network allows displacement calculation between any two acquisitions, regardless of the possibility of generating a particular interferogram. We apply a temporal coherence threshold to the final time-series, calculated using the formulation by Gourmelen et al. (2010), to eliminate bias from phase-unwrapping. We select only pixels characterized by a temporal coherence greater than 0.7, a typical value in InSAR applications (Borgia et al., 2005; Casu et al., 2006; Chaussard & Amelung, 2012; Tizzani et al., 2007). We also apply DEM correction after the inversion of the network of interferograms to remove the dependence of the displacement history to the perpendicular baseline history (Fattahi & Amelung, 2013). We do not use spatio-temporal filtering to remove atmospheric effects because of the small number of scenes in our time-series and because atmospheric effects are small compared to the high deformation rates observed.

4. Results: Time-series reveal subsidence in twenty-one locations

A map of the averaged LOS velocity identifies actively deforming areas (Fig. 2). Positive LOS velocities (blue colors) represent movement towards the satellite (e.g. uplift); negative LOS velocities (red colors) represent movement away from the satellite (e.g. subsidence). We evaluate, based on the variance of the time dependent displacements, that the detection threshold for the entire survey is ±2 cm/yr (green–yellow colors in Fig. 2) and varies depending on the number of SAR acquisitions and atmospheric conditions. In cities this threshold decreases because of the lack of significant topography and associated atmospheric delays.

We detect land subsidence in a total of 21 locations (Fig. 2, black diamonds), 17 of which occur in or nearby urban areas, from east to west: Puebla, Mexico City (and greater metropolitan area, such as Ciudad Netzahualcoyotl), Toluca, Queretaro, San Luis de la Paz, San Luis Potosi, Morelia, Celaya, Salamanca, Irapuato, Silao, Leon, Aguascalientes, Zamora, Guadalajara, Ahuacatlan, and Tepic. The remaining 4 subsiding locations are agricultural areas outside major urban centers: 20 km southwest of the city of San Luis de la Paz near the village of El Paredon, south of Villa de Reyes (40 km south of San Luis Potosi), west of Villa de Arista (50 km north of San Luis Potosi), and in the graben between Aguascalientes and Luis Moya.

4.1. Horizontal and vertical deformation

The limitation of ALOS is that mostly ascending acquisitions are available; thus vertical and horizontal components of the deformation cannot be retrieved independently. The only urban area for which ascending and descending viewing geometries are available is Mexico City. There we retrieve the 2-D deformation field following the approach of Wright, Parsons, and Lu (2004). Fig. 3 shows the horizontal and vertical ground displacement obtained by combining 19 ascending acquisitions with 5 descending acquisitions. Because descending acquisitions have long temporal baselines (8 months in average) the descending averaged velocity map suffers from coherence loss, which is transmitted to the vertical and horizontal averaged velocity maps. Nevertheless, the results confirm that the horizontal ground displacement is minimal compared to the vertical contribution. These results are in agreement with studies based on GPS and other InSAR data in Mexico City, which indicate that 85–90% of the 3-D displacement vectors is vertical (e.g. Cabral-Cano et al., 2008; López-Quiroz et al., 2009; Ortiz-Zamora & Ortega-Guerrero, 2010; Osmanoglu et al., 2011; Strozzi & Wegmuller, 1999; Yan et al., 2012).

Following this observation and because InSAR is more sensitive to vertical than horizontal movements we convert LOS (d_{LOS}) into vertical displacement (d_v) for every SB time-series using the ALOS incidence angle ($\theta = 34.3°$): $d_v = d_{LOS}/\cos\theta$. Vertical ground displacement is 21% more than LOS displacement, i.e., 1 cm of LOS displacement corresponds to 1.2 cm of vertical displacement. In the rest of this paper we use vertical subsidence rates converted from the observed LOS rates. The borders of the subsiding areas may however present significant horizontal deformation due to the high velocity gradients.

4.2. Categories of land subsidence

Although each subsidence site is unique, as it reflects local geological and hydrological conditions, we found similarities between sites, which allow us to classify detected subsiding locations into characteristic

Table 1
ALOS PALSAR scenes processed to study city subsidence in central Mexico. The major cities (>100,000 inhabitants) covered by each track are shown in the last column.

Track number	Frame numbers	Earliest scene	Latest scene	Number of scenes	Number of igrams	Cities > 100 000 inhabitants
181	370–380	18 Feb 2007	14 Jan 2011	12	24	Veracruz
182	370–380	23 Jul 2007	31 Jan 2011	12	26	Xalapa
183	360–370	06 Feb 2007	02 Jan 2011	11	16	
184	370	26 Aug 2007	19 Jan 2011	13	27	Puebla
185	370	28 Jul 2007	21 Dec 2010	11	21	Puebla
186	370	11 Feb 2007	07 Jan 2011	19	47	Mexico City
187	370–380	28 Feb 2007	09 Dec 2010	13	26	Toluca
188	370–440	02 Aug 2007	10 Nov 2010	14	33	Queretaro, San Luis Potosi
189	380–430	04 Oct 2007	27 Feb 2011	8	15	Celaya, San Luis Potosi
190	380–430	05 Mar 2007	16 Mar 2011	11	22	Morelia, Irapuato, Leon
191	380–430	22 Mar 2007	02 Apr 2011	19	43	Aguascalientes
192	380–400	24 Aug 2007	04 Mar 2011	16	31	
193	380–400	26 Jul 2007	03 Feb 2011	12	27	
194	380–400	12 Aug 2007	20 Feb 2011	14	24	Guadalajara
195	370 & 410	26 Feb 2007	22 Jan 2011	15	31	Colima
196	410	30 Apr 2007	24 Dec 2010	13	28	Tepic

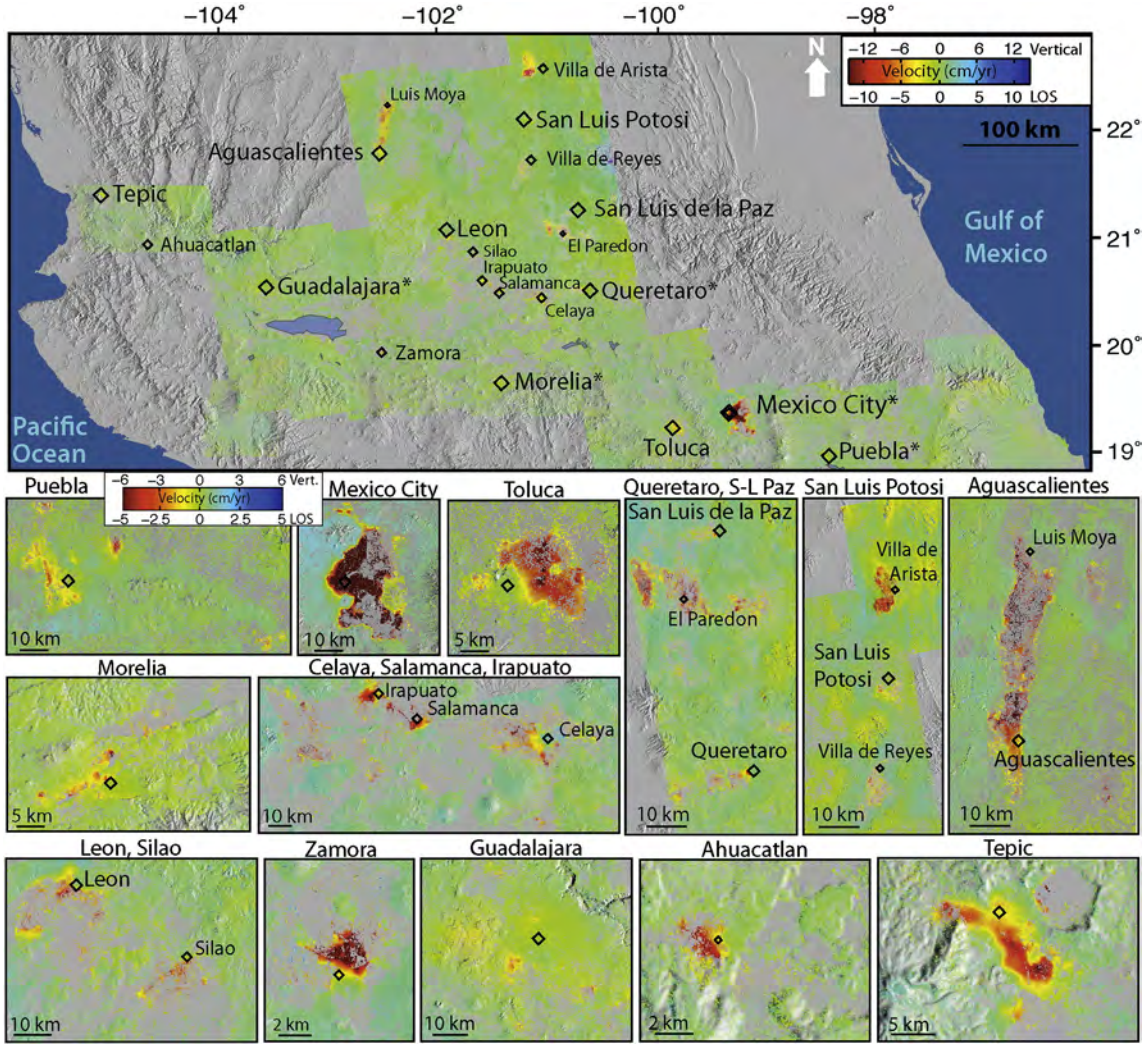

Fig. 2. Averaged 2007–2011 LOS velocity map of central Mexico from ALOS InSAR time-series analysis, overlaying SRTM V4 shaded topography. The color scale shows red colors as negative LOS velocities (subsidence) and blue colors as positive LOS velocities (uplift). Vertical subsidence rates converted from the LOS rates are labeled on the color scale. The emplacement of the 21 subsiding locations are shown by black diamonds and labeled for reference; cities included in the UNESCO World Heritage list are marked by an asterisk. 17 subsiding cities are observed (from east to west): Puebla (population of 2.5 million), Mexico City and associated urban area, such as Ciudad Netzahualcoyotl (population of 21 million), Toluca (population of 427,000), Queretaro (population of 825,000), San Luis de la Paz (population of 101,000), San Luis Potosi (population of 936,000), Morelia (population of 537,000), Celaya (population of 266,000), Salamanca (population of 144,000), Irapuato (population of 317,000), Silao (population of 147,000), Leon (population of 1.4 million), Aguascalientes (population of 735,000), Zamora (population of 186,000), Guadalajara (population of 3.8 million), Ahuacatlan (population of 6.5,000), and Tepic (population of 261,000). 4 subsiding locations are outside cities: southwest of San Luis de la Paz near El Paredon, south of Villa de Reyes, west of Villa de Arista, and between Aguascalientes and Luis Moya. The bottom insets display zooms of the subsiding areas with a smaller color scale, grouped based on their geographical proximity, and organized from east to west (with the exception of Aguascalientes). (For interpretation of the references to color in this figure legend, the reader is referred to the web version of this article.)

categories. We describe the subsiding sites according to four main criteria (Table 2) similar to Chaussard, Amelung, Abidin, and Hong (2013): (1) the rates of subsidence (less or more than 5 cm/yr); (2) its spatial extent (large-scale: ≥100 km^2, local: 10–100 km^2, or patchy: <10 km^2), both deduced from the averaged ground velocity maps (Figs. 3–9 and Supplementary Material Figs. S1–19); (3) the correlation between velocity gradients and locations of existing faults; and (4) the type of land use (agricultural, urban, or industrial).

As mentioned in Section 2, decline in pore-water pressure related to groundwater extraction likely controls the emplacement of land subsidence (e.g., location of the major wells). However, because of the large extent of the study area and the difficulty in accessing water extraction bookkeeping records from different local water management agencies (Rodríguez, Lira, & Rodríguez, 2012), we are not able to precisely address the contribution of each extraction well to the observed subsidence. Instead we utilize land use as a proxy for the general amount of groundwater extracted: groundwater use is first agricultural (77%), second urban (13%), and third industrial (10%) (CNA, 2004). We rely on Google Earth optical imagery to classify land use: green colors and geometric patterns indicate agricultural land use, small habitations and brown or gray colors indicate urban land use, and larger buildings with white roofs indicate industrial land use (see kmz files provided with this paper and Supplementary Material Fig. S1–19, mixed land use is urban and industrial).

Because groundwater extraction is widespread we also address the other parameters that may influence the location of subsidence. We test for fault control by examining whether changes in subsidence rates occur across mapped faults (Servicio Geologico Mexicano, 1998) and consider the influence of the surface geology. As most groundwater-related subsidence occurs in compressible deposits (alluvium and lacustrine deposits), we isolate the exceptions: subsidence in intermediate (lahars and sandstone) or incompressible (basalt, andesite, rhyolite, and limestone) deposits, and examine whether surface geology contours coincide with limits of the subsiding areas. Finally, we qualitatively estimate if the fastest subsidence coincides with the thickest sediments, i.e. if it occurs in the basin or graben depocenter.

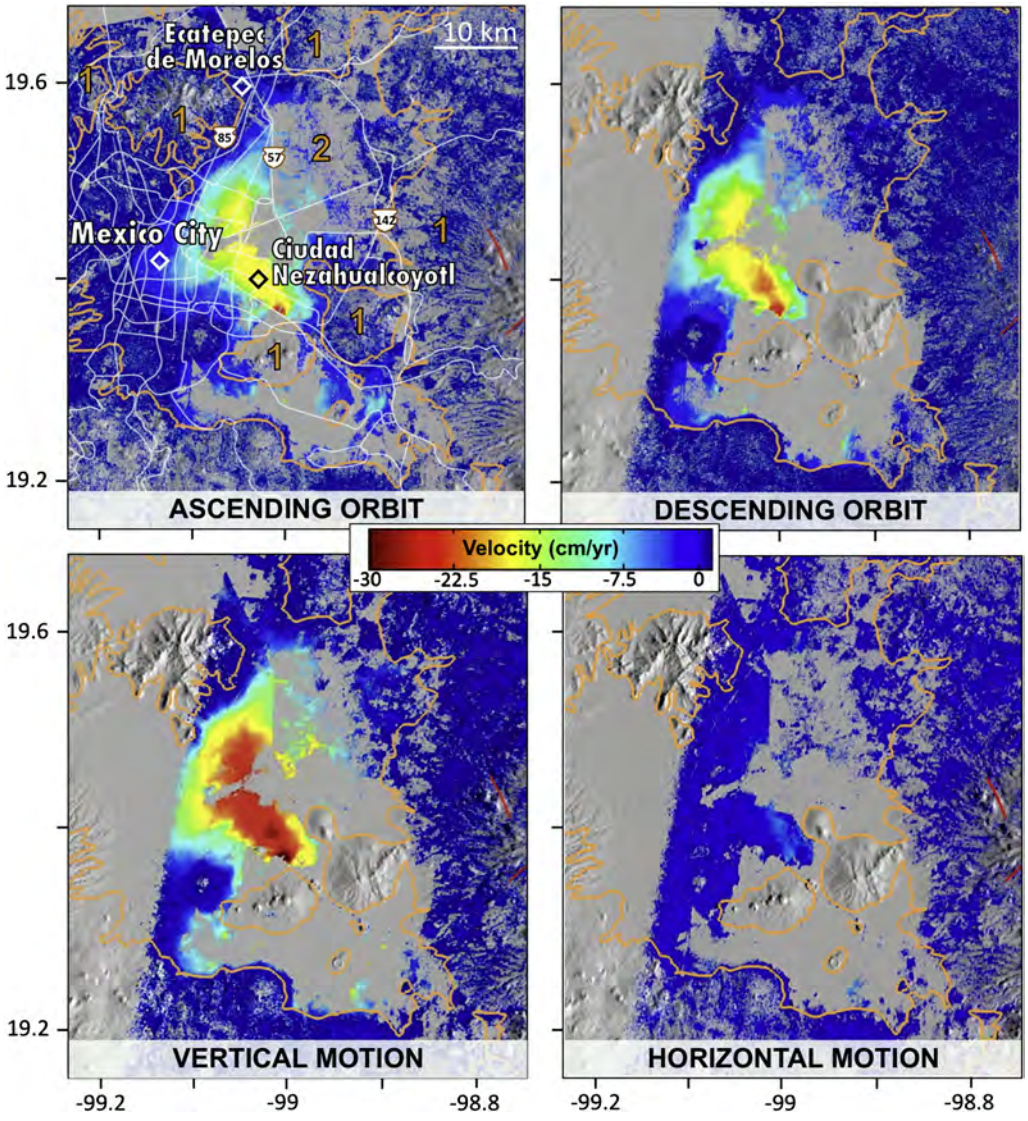

Fig. 3. Average 2007–2011 velocity maps of Mexico City. The 2-dimensional velocity field is extracted using ascending and descending acquisitions. Roads are shown with white lines and main towns are marked by diamonds and labeled for reference on the top left map. Surface geology contours are shown in light brown and referred to using brown numbers (primarily compressible, intermediate, and incompressible deposits are labeled 2, 3, and 1 respectively), faults are shown by red lines (derived from the Geologic-Mining maps of Mexico, Servicio Geologico Mexicano (1998)). We confirm that horizontal ground displacement is minimal. (For interpretation of the references to color in this figure legend, the reader is referred to the web version of this article.)

Using these criteria we separate 3 main categories of subsidence: rapid and large-scale, rapid and local scale, and slow and patchy. The two first categories include subcategories based on the influence of existing faults. One representative example illustrating each case is presented in Figs. 4–9. Similar figures, including Google Earth imagery, are shown for all the subsiding locations in the supplementary material. Figs. 4–9 are organized as follows: (a) shows the averaged velocity map, the surface geology (brown contours and numbers, primarily compressible, intermediate, and incompressible sediments are labeled 2, 3, and 1 respectively), and the fault traces (red lines); (b) shows the vertical displacement time-series in locations with rapid subsidence; and (c) when applicable, show velocity profiles across faults in the vicinity of subsiding areas. Observations from these figures are summarized in Table 2 and are used in the Discussion section to evaluate the causes and parameters influencing land subsidence at each site.

The first observation from Figs. 4–9(b) is that in every location subsidence occurs at nearly constant rates over the 4-yr period spanned by the SAR acquisitions. The subsidence rates are evaluated using linear regressions to limit the effect of atmospheric phase delay that may affect certain acquisitions. The precision of the subsidence rates is ~1 cm/yr, based on the variability of the linear fit through the time-series. Lower subsidence rates suffer from larger scattering due to proportionally larger atmospheric contributions (e.g. Fig. 9 compared to Fig. 4).

4.2.1. Category 1: Rapid, large-scale subsidence

This category groups locations where subsidence ≥5 cm/yr is taking place at large-scale (>100 km^2). We differentiate 2 subcategories:

A) Fault-limited

This category includes the subsiding locations between Aguascalientes and Luis Moya (covering ~500 km^2 and reaching ~8 cm/yr, Fig. 4(a)), south of San Luis de la Paz (covering ~240 km^2 and reaching ~9 cm/yr), and south of Villa de Reyes (covering ~100 km^2 and reaching ~5 cm/yr). In all these locations high velocity gradients correlate with mapped faults: the western and eastern limits of the subsiding area north of Aguascalientes present a velocity gradient of 2 cm/yr over ~1.5 km (Fig. 4(c) blue and pink profiles) and the eastern and western limits of the areas south of San Luis de la Paz and south of Villa de Reyes show similar gradients over ~1 km, all correlating with pre-

Table 2
Summary of observations in the 21 subsiding areas: category (spatial extent and rate, column 2), maximum subsidence rate (column 3), correlation between velocity gradients and locations of pre-existing faults (column 4), relation with land use (column 5, agri: agricultural, indust: industrial), type of sediments experiencing subsidence (column 6), and correlation between changes in sediment types or thicknesses and changes in subsidence rates (column 6, correlation Yes/No). The horizontal bold lines separate different categories and subcategories. A gray font highlights variations within a given subcategory, as described in the text. The long-term temporal variability is isolated from comparison with previous works as described in Section 5.1 (column 7).

Locations	Category	Max rate (cm/yr)	Correlation with faults	Land use	Sediment type/ correlation with changes in sed. type or with thickness (Y/N)	Long-term temporal variability
North Aguascalientes (Fig. 4)	Rapid, large-scale (1)	8.3	Fault-limited	Agri.	Compressible/ Y (type)	n/a
South of S.-L. de la Paz		8.8				
West of Villa de Reyes		5.2				
Mexico City (Fig. 2)		30.0	Not fault-limited	Urban	Compressible/ Y (thickness)	N
Toluca (Fig. 5)		7.0				
West of Villa Arista		18.4		Agri.	Compressible/N	n/a
Queretaro (Fig. 6)	Rapid, local-scale (2)	5.0	Fault-limited	Urban	Compressible/N	Y
Morelia		6.7				N
Salamanca		7.4				n/a
Aguascalientes (Fig. 4)		5.5		Urban	All types	Y
Irapuato		7.2			Comp. & intermediate	n/a
Celaya		8.5		Agri.	Compressible/N	Y
Silao		5.0				n/a
Leon		5.2				
Tepic (Fig. 7)		6.8	Not fault-limited	Urban	Compressible/N	n/a
Zamora		12.8				
Ahuacatlan		5.0				
S.-L. Potosi (Fig. 8)	Slow, patchy (3)	3.9	Not fault-limited	Urban	Compressible/N	n/a
S.-L. de la Paz		4.0		Indust.	Incompressible	n/a
Guadalajara (Fig. 9)		3.3			All types	
Puebla		4.4				

existing early Oligocene faults (Nieto-Samaniego, Alaniz-Álvarez, & Camprubí, 2007). Note that in these locations faults coincide with transitions between compressible and incompressible deposits. In these three sites subsidence occurs in agricultural land use.

B) Not fault-limited
This category includes the subsiding areas in Mexico City, in Toluca, and west of Villa de Arista where subsidence is occurring at rates up to 30, 7, and 18 cm/yr and is covering ~500, ~150, and ~220 km^2, respectively (Figs. 2 and 5(a)). There are no pre-existing faults at the transition between stable and subsiding areas. In Mexico City and Toluca, subsidence is associated with urban land use and is located in the center of the sedimentary basin (Figs. 2 and 5(a)). West of Villa de Arista, subsidence is associated with agricultural land use and does not correlate with the basin depocenter.

4.2.2. Category 2: Rapid, local-scale subsidence

This category groups locations where subsidence ≥5 cm/yr is taking place at local-scales (10–100 km^2). We differentiate 2 subcategories:

A) Fault-limited
This category includes Queretaro, Morelia, Salamanca, Aguascalientes, Irapuato, Celaya, Silao, and Leon. In Queretaro (Fig. 6), Morelia, and Salamanca subsidence up to 5, 7, and 7 cm/yr occurs in ~20 km^2 areas in the northwest, north, and northwest of the cities, respectively; in Aguascalientes a 100 km^2 area with subsidence up to ~6 cm/yr occurs in the center, and higher rates in the north (Fig. 4(a)); in Irapuato a 45 km^2 area of subsidence up to ~7 cm/yr occurs in southwest of the city; and in Celaya, Silao, and Leon subsidence up to 9, 5, and 5 cm/yr occurs in 75 km^2 areas in the south and east, south, and south of the city centers, respectively. In all these location pre-existing Cenozoic faults correlate with the limits of the subsiding areas, velocity gradients of 2 cm/yr being observed on a distance <1 km (Fig. 4(c) gray profile and 6(c)). In the first five locations subsidence correlates with urban land use, while in the last three subsidence correlates with agricultural land use. In central Aguascalientes and in Irapuato, subsidence is not limited to compressible deposits: in Aguascalientes subsidence occurs in all three types of deposits (compressible, intermediate and incompressible) (Fig. 4(a)), and in Irapuato in two (compressible and intermediate).

B) Not fault-limited
This category includes Tepic, where 20 km^2 of subsidence at up to ~7 cm/yr occurs in the southern part of the city (Fig. 7(a)), Zamora, where 15 km^2 of subsidence at up to ~13 cm/yr occurs in the north part of the city, and Ahuacatlan, where subsidence at ~5 cm/yr is observed all over the urban area, the smaller spatial extent being related to the small surface area of the city. In all these locations

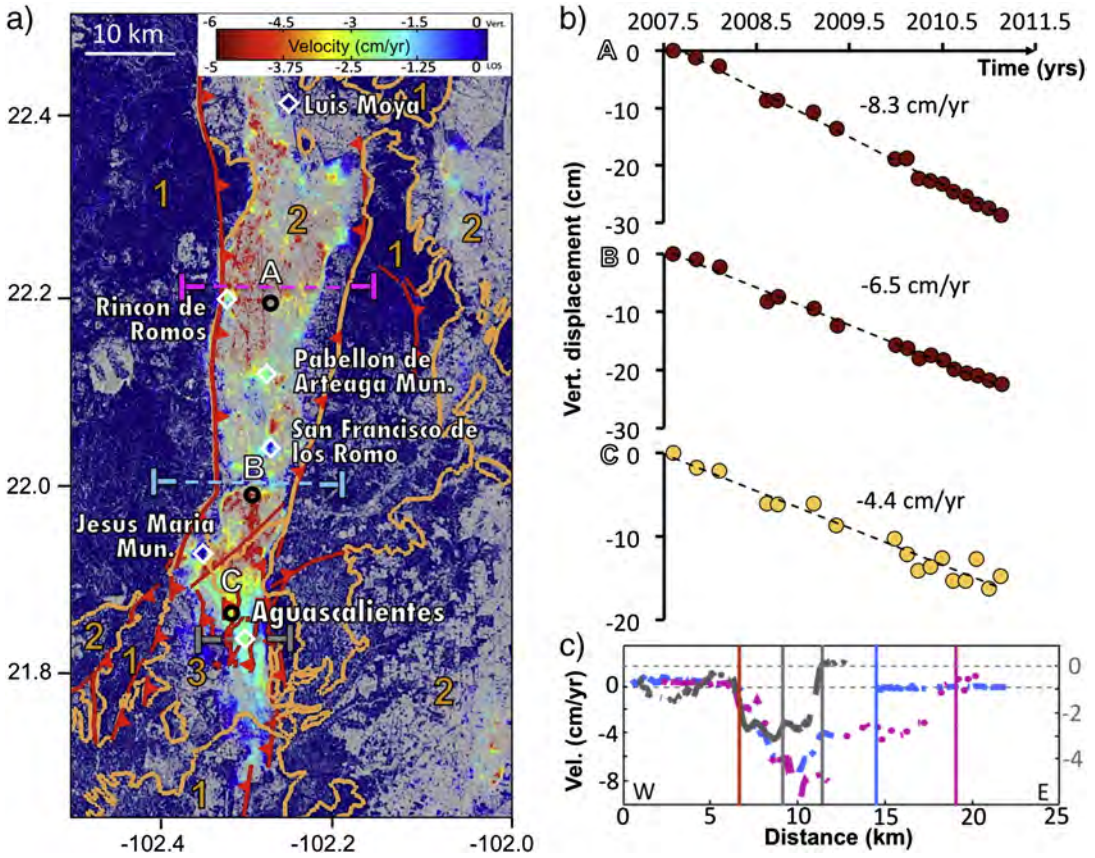

Fig. 4. Subsidence in the city of Aguascalientes and the Aguascalientes graben. Subsidence throughout the Aguascalientes graben illustrates category 1 in the case where the boundaries of the subsiding areas are fault-limited and coincide with transition in sediment types. The subsidence in the city illustrates category 2 in the case where the limits of the subsiding areas are fault-limited and the subsidence is not limited to compressible deposits. a) Average 2007–2011 velocity map with the same legend as Fig. 2 (roads are not shown for readability). Black circles show the location of the pixels whose time-series are showed in b). b) Vertical displacement time-series and corresponding linear rates of subsidence. c) Velocity profiles across pre-existing faults in the vicinity of subsiding areas. The locations of the profiles are denoted by dashed colored lines on (a). The locations of the faults intersecting each profile are noted in the same color as the profile itself or in red in common to all profiles. (For interpretation of the references to color in this figure legend, the reader is referred to the web version of this article.)

subsidence correlates with urban land use and velocity gradients do not correlate with the locations of existing faults.

4.2.3. Category 3: Slow and patchy subsidence

This category groups locations where subsidence is taking place at low rates (<5 cm/yr), on a smaller spatial scale, and is not bordered by pre-existing faults. It includes San Luis Potosi, San Luis de la Paz, Guadalajara, and Puebla. In San Luis Potosi (Fig. 8) and San Luis de la Paz subsidence reaches a maximum of ~4 cm/yr in 2 patches; in Guadalajara subsidence up to ~3 cm/yr is observed in 2 patches (Fig. 9(a)); and in Puebla subsidence up to ~4 cm/yr is observed in 3 patches. In the first two locations subsidence correlates with urban land

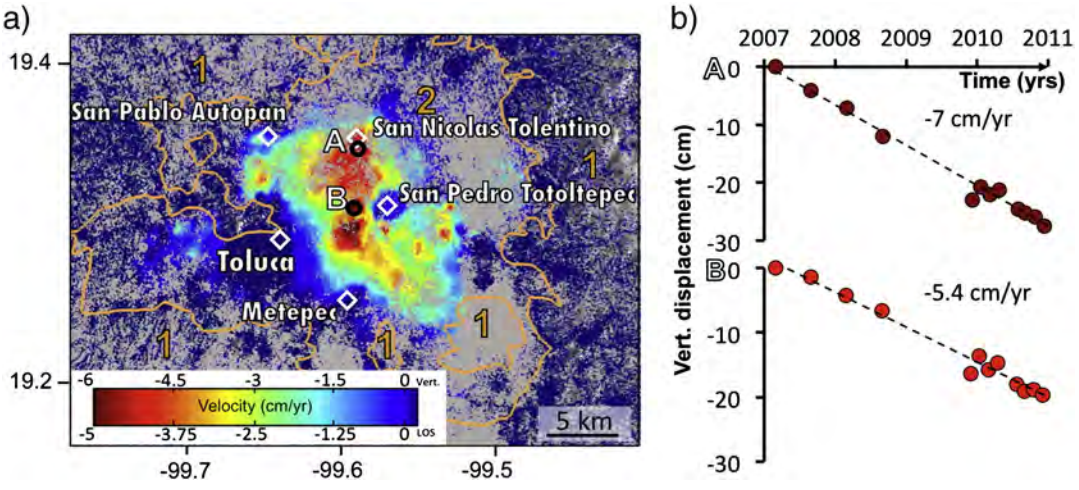

Fig. 5. Same as Fig. 4 for Toluca, which illustrates category 1 in the case where the subsidence is not fault-limited, and the maximum subsidence correlates with the sediment thickness. (For interpretation of the references to color in this figure, the reader is referred to the web version of this article.)

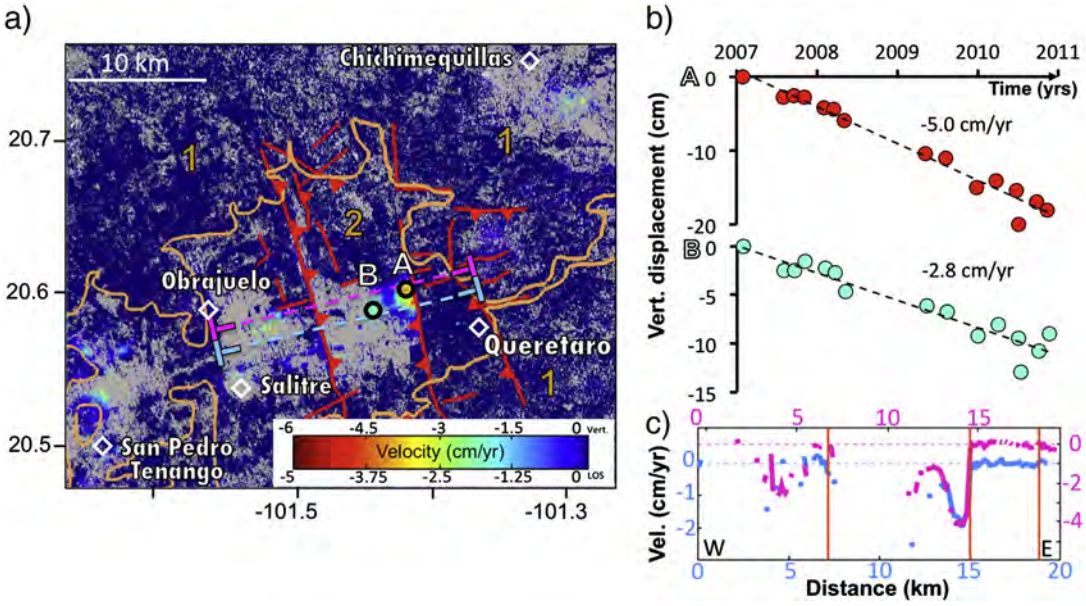

Fig. 6. Same as Fig. 4 for Queretaro, which illustrate category 2 in the case where the subsidence is fault-limited. (For interpretation of the references to color in this figure, the reader is referred to the web version of this article.)

use and occurs in compressible deposits, while in the last two subsidence correlates with industrial land use and also occurs in intermediate and incompressible deposits.

5. Discussion

5.1. Comparison with previous studies and long-term temporal variability of the subsidence

While the linear subsidence rates observed during our 4 yrs of observations suggest a temporal consistency over short time scales, comparison with previous studies allows us to evaluate the variability of the rates and spatial distribution of land subsidence over longer time scales. Seven of the twenty-one subsiding areas have been previously studied using observations until up to 2010. We present the cities from east to west, following the observations of Fig. 2 and discuss the long-term temporal variability of land subsidence. Only differences higher than the precision of our subsidence rates (1 cm/yr) are considered significant.

Many previous land subsidence studies focused on Mexico City. Earliest work relied on leveling (Vega, 1976; Mazari & Alberro, 1991; and references therein) and piezometers (Ortega-Guerrero, Rudolph, & Cherry, 1999; Vega, 1976), while more recent surveys used GPS (Cabral-Cano et al., 2008) and InSAR (Cabral-Cano et al., 2008; Cabral-Cano, Osmanoglu, et al., 2010a; Cabral-Cano, Arciniega-Ceballos, et al., 2010b; López-Quiroz et al., 2009; Osmanoglu et al., 2011; Strozzi & Wegmuller, 1999; Strozzi, Wegmuller, Werner, Wiesmann, & Spreckels, 2003, Strozzi, Werner, Wegmuller, & Wiesmann, 2005; Yan et al., 2012). The earliest studies suggested subsidence up to 50 cm/yr in the historic downtown area between 1940 and 1960, while later work provided

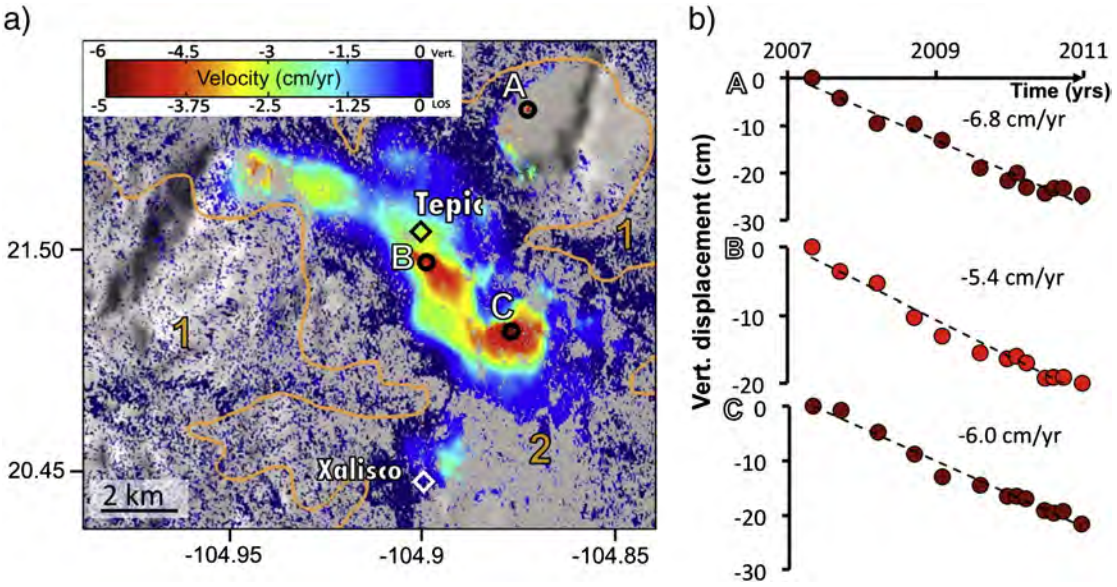

Fig. 7. Same as Fig. 4 for Tepic which illustrate category 2 in the case where the subsidence is not fault-limited. (For interpretation of the references to color in this figure, the reader is referred to the web version of this article.)

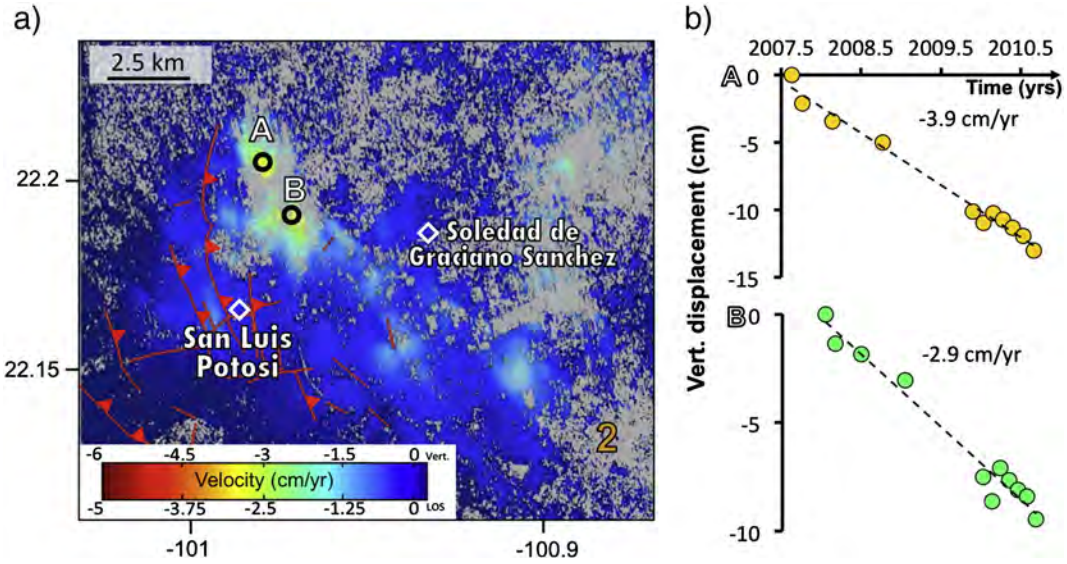

Fig. 8. Same as Fig. 4 for San Luis Potosi which illustrate category 3 in the case where the subsidence patches are located in compressible deposits. (For interpretation of the references to color in this figure, the reader is referred to the web version of this article.)

lower estimates, up to 30–35 cm/yr in 2002–2007 in the eastern sector of the city, the central part of Ciudad Nezahualcoyotl. The rates of 30 cm/yr and the spatial distribution of land subsidence observed in our 2007–2011 survey are in good agreement with these works.

In Toluca 2003–2008 Envisat InSAR data revealed subsidence up to 8 cm/yr in the industrial corridor east of the city center (Calderhead, Martel, Alasset, Rivera, & Garfias, 2010, Calderhead, Therrien, Rivera, Martel, & Garfias, 2011), in agreement with our 2007–2011 spatial distribution and rates of 7 cm/yr.

In Queretaro 2003–2006 Envisat InSAR data revealed land subsidence up to 7 cm/yr south of the city center (Farina, Avila-Olivera, Garduño-Monroy, & Catani, 2008, Farina et al., 2007). Our observations agree with the spatial distribution but our rates of 5 cm/yr are lower.

Morelia has been frequently studied using Envisat InSAR (Cigna et al., 2011, 2012; Farina et al., 2007, 2008). All studies agree that the maximum subsidence is taking place in the footwall of the northernmost faults, consistent with our observations. Farina et al. (2007, 2008) detected subsidence up to 3.5 cm/yr using 2003–2006 interferograms, while Cigna et al. (2011, 2012) showed subsidence rates up to 7–8 cm/yr during 2003–2010 using PS-InSAR time-series. Our estimates are in agreement with the latest, suggesting constant subsidence at ~7 cm/yr, the rate of 3.5 cm/yr being likely an underestimation maybe related to unwrapping issues.

In Celaya 2003–2006 Envisat InSAR revealed maximum subsidence in the middle of the urban area (Avila-Olivera et al., 2008; Farina et al., 2007, 2008) with rates varying from 2 to 3 cm/yr in the first two studies to 7–10 cm/yr in the latter. Our 2007–2011 observations are consistent with the highest subsidence rates (9 cm/yr) suggesting that, similar to the case of Morelia, subsidence is likely constant and the rates of 2–3 cm/yr are underestimations. However, the spatial distribution of

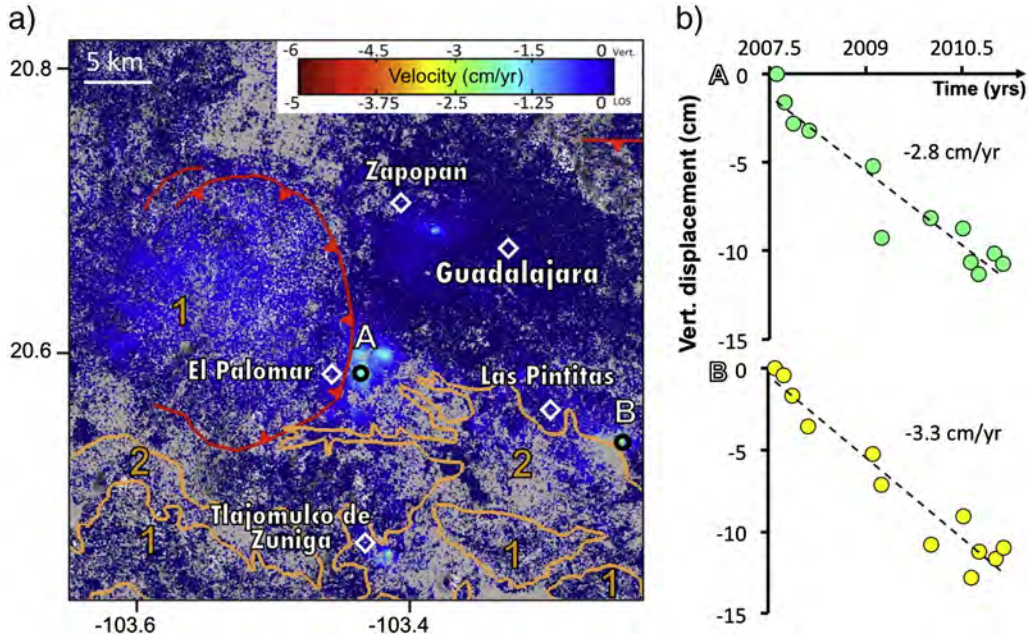

Fig. 9. Same as Fig. 4 for Guadalajara which illustrate category 3 in the case where the subsidence patches are not located in compressible deposits. (For interpretation of the references to color in this figure, the reader is referred to the web version of this article.)

subsidence differs: we detect only small subsidence in the city center, the maximum deformation occurring west and south of it.

In Aguascalientes 2003–2008 Envisat InSAR data revealed up to 7 cm/yr of subsidence in the city and 12 cm/yr in the north of the urban area (Cigna et al., 2011). These rates are higher than the 5.5 and 8.3 cm/yr observed during our 2007–2011 survey in the city and in the north, respectively.

In Irapuato, Castillo and Aguirre (2010) and Schroeder and Rodríguez (2010) used 2000–2010 GPS and leveling data to detect subsidence up to 1.4–2.5 cm/yr (without specifying the location). Despite the overlapping time coverage we detect significantly higher rates (up to 7 cm/yr) in the southwest of the city. This disparity likely reflects the limitations of point-based surveys.

In summary, in Mexico City, Toluca, and Morelia subsidence rates and spatial distribution have remained unchanged for at least the past 1–2 decades, suggesting a well-established system and a consistency in the causes of subsidence. The subsidence rates are likely representative of the amount of water extracted and the thickness of the compressible deposits. On the other hand, in Celaya the spatial distribution is shifting while in Aguascalientes and Queretaro subsidence rates change through time. This suggests more variable systems in which the activities performing groundwater extraction are changing spatially and temporally.

5.2. Causes of subsidence

Based on the rates, spatial patterns, and relations between subsidence and land use we evaluate the processes responsible for the observed subsidence. The rapid subsidence rates of 5–30 cm/yr cannot be explained by natural processes such as isostatic sediment loading or consolidation of Holocene deposits with typical rates of a few mm/yr (Dixon et al., 2006; Meckel, Brink, ten, & Williams, 2006; Teatini, Tosi, & Strozzi, 2011). The anthropogenic process evoked to explain land subsidence in Mexico is groundwater extraction in cities and agricultural centers (e.g. Carreón-Freyre, Cerca, Luna-González, and Gámez-González (2005) and references therein; Galloway and Burbey (2011)). We explore the possibility of other anthropogenic processes, such as changes in surface water drainage or mining activities, causing the observed land subsidence.

Most Mexican cities were already developed in the 1800 s when Mexico gained its independence from Spain and are intensely populated since the 1970's (Alba, 1982). Thus, it is unlikely that changes in surface water drainage and artificial sediment loading, processes usually resulting in subsidence in the first decades after land modification (Mazzotti, Lambert, Van der Kooij, & Mainville, 2009; Sestini, 1996; Yan & Gong, 2002), are responsible for the observed subsidence. Although mining is widespread in Mexico (Sánchez-Mejorada, 2000), optical images reveal the occurrence of mining sites in only one subsiding area (south of Aguascalientes, Supplementary material Fig. S10 inset C) and in any case these activities are extremely localized and don't have the extent detected. Oil and gas fields are located only on the eastern coast of Mexico (Valera & Stange, 2011) and do not correlate with any of the observed subsidence areas. Thus, most of the detected subsiding areas in central Mexico are the result of groundwater extraction.

We infer the type of groundwater extraction responsible for subsidence from the land use (Table 2). The subsiding areas north of Aguascalientes, south of San Luis de la Paz, south of Villa de Reyes, west of Villa de Arista, in Celaya, Silao, and Leon are agricultural, suggesting that land subsidence is due to groundwater pumping for agricultural activities. The subsiding areas in Mexico City, Toluca, Queretaro, Morelia, Salamanca, center Aguascalientes, Irapuato, Tepic, Zamora, Ahuacatlan, San Luis de la Paz, and San Lusi Potosi are urban, suggesting that subsidence is due to groundwater pumping for urban activities. In Guadalajara and Puebla land subsidence is likely due to groundwater pumping for industrial activities.

5.3. Role of surface geology and pre-existing faults

We discuss how the combination of groundwater withdrawal, stratigraphic, and structural features (distribution of lithostratigraphic units and pre-existing faults) may influence the spatial and temporal distributions of land subsidence.

5.3.1. Surface geology

Most locations experiencing rapid land subsidence are located on compressible or intermediate deposits (alluvium or lacustrine deposits and lahars or sandstone) (Table 2). The only three exceptions being small patches of subsidence observed south of Aguascalientes, in Guadalajara, and in Puebla. In Aguascalientes the subsidence south of the city in rhyolitic deposits is correlated with mining activities (Supplementary material Fig. S10 inset C) while in Guadalajara and Puebla the subsidence patches correlate with industrial activities (Fig. 9 inset A, Supplementary material Figs. S18 and S19). These observations suggest that the subsidence either results from consolidation of deep compressible units (pumping of confined aquifers) or that local variations in surface geology exist but are not included in the regional geologic maps (local compressible sediment being present but not documented).

Three cities with over 100,000 inhabitants covered by our survey do not present land subsidence: Colima, Xalapa, and Veracruz (Fig. 1). The absence of subsidence in the first two can be related to the lack of compressible deposits, Colima and Xalapa being characterized by volcanic basements. On the opposite Veracruz is developed on compressible lacustrine and eolian deposits but the aquifers are not overexploited, possibly explaining the absence of subsidence there (Scott, Dall'erba, & Caravantes, 2010).

In five locations we notice a correlation between changes in sediment facies and the boundaries of the subsiding areas (Table 2). In three of these locations changes in surface geology also correlate with the location of existing faults, thus the limits of the subsiding areas are likely controlled both by the existing faults and the sediment distribution (north of Aguascalientes, south of San Luis de la Paz, and south of Villa de Reyes). In the remaining two locations we observe a correlation between the expected thickness of compressible deposits and the location of land subsidence (Mexico City and Toluca). In these two cities groundwater extraction has been occurring for a prolonged period of time. Thus, the rates and spatial patterns of subsidence are likely controlled by the continuous overexploitation of the aquifers and the thickness of the compressible deposits: thicker deposits result in greater subsidence rates and larger patterns where intense groundwater extraction is performed. The significantly higher rates and larger pattern of subsidence observed in Mexico City illustrate this concept. Mexico City is located in a lacustrine basin overlaying an aquifer system up to 500 m thick (Ortega-Guerrero et al., 1999), whereas other subsiding locations are located in intramontane basins with a sediment thickness of only tens to 200 m (e.g. Calderhead et al., 2011; Cigna et al., 2011; Huizar-Álvarez et al., 2011).

5.3.2. Faults as barriers to subsidence and groundwater flow

One of the most significant observations from the averaged velocity maps is the identification of high gradients of ground velocities. In all the locations we notice that light blue colors, corresponding to the transition between subsiding and stable areas are occurring on narrow zones (<2 km wide) (as seen for example in Fig. 4(a)). Because hazard assessments depend on horizontal velocity gradients (Cabral-Cano, Diaz-Molina, & Delgado Granados, 2011; Cabral-Cano, Osmanoglu, et al., 2010; Cabral-Cano et al., 2012; Cigna et al., 2011), our observations emphasize the high risk of damages associated with land subsidence throughout Mexico.

Traditionally the lateral transition of sediment facies is gradual and so are the displacements associated with their consolidation. Thus, the detection of abrupt changes in ground displacement suggests the presence of mapped or unmapped faults. In eleven locations pre-existing

geologic faults correlate with the high velocity gradients (Table 2). But because some fault traces may be difficult to identify in the field unmapped faults may also be present in many other locations where high velocity gradients are detected. The deformation pattern detected by InSAR in early stages subsidence systems can be used to map new faults or identify regions where fracture systems are likely to develop (e.g. Cabral-Cano, Osmanoglu, et al. (2010a)), such as for example in Tepic (Figs. 4 and 7(a)) where high differential ground motion is occurring with a limited spatial extent.

Laterally adjacent lithologic units juxtaposed by faulting can have different properties (compressibility and permeability), thicknesses, and water level changes (e.g. Maclay & Small, 1983); thus these units have different subsidence potentials. Subsidence is systematically observed on the footwall of the faults (e.g. Fig. 4), where sediments are thicker, in agreement with a greater subsidence potential (Cigna et al., 2011; Pacheco et al., 2006). Because of the high differential velocities observed (several centimeters per year) and the small spatial extent of the displacement compared to the fault lengths, we suggest that the motion on the faults is driven by water extraction rather than by tectonic activity (example in Figs. 4 and 6(c)). Subsidence induced faulting mimics the location of older (tectonic) faults even though their driving forces are different. In some cases, such as in Morelia, it is possible that a tectonic component is also added to the subsidence signal (Cabral-Cano, Arciniega-Ceballos, et al., 2010; Cigna et al., 2012).

Faults are known to act either as low-permeability barriers or as conduits to fluid flow (e.g. Caine, Evans, & Forster, 1996). In Mexico they coincide with limits of the subsiding areas and thus likely serve as barriers to groundwater flow and partition the aquifer systems at depths. The development of gouge material along fault planes by grain size reduction and the different properties of the lithologic units juxtaposed by faulting likely explain this behavior (Teufel, 1987). Similar observations have been made by Cigna et al. (2012) in Morelia who suggested that faults act as a barrier to groundwater flow in the perpendicular direction, whereas water flow along the faults is increased. Further study of subsiding areas bordered by faults could improve our knowledge of the spatial heterogeneity in structure and material properties of the aquifer systems, important parameters for the development of high-resolution groundwater flow models.

5.4. Lack of seasonal effects

The linearity of the deformation during the 4 yrs covered by our survey likely reflects a consistency in the cause of subsidence, i.e. groundwater extraction is continuous and at nearly constant rates. Our survey did not reveal seasonal variability at any of the subsiding areas. Although the sensitivity of ALOS for seasonal deformation is limited because of the temporal sampling (46 days), seasonal variations should be detectable as data during both dry and rainy seasons were acquired. This lack of strong seasonal variability, also confirmed by GPS data in Mexico City (Osmanoglu et al., 2011), is in opposition to observations of subsidence in the western United States where faults have also been documented as impeding horizontal propagation of fluid-pressure changes but mainly on seasonal scales (Amelung, Galloway, Bell, Zebker, and Laczniak, 1999, in Las Vegas; Bawden, Thatcher, Stein, Hudnut, and Peltzer, 2001 in the Los Angeles Basin; and Schmidt and Bürgmann, 2003, in the Santa Clara valley).

The presence or absence of seasonal effects can help identify the source of subsidence within an aquifer system. Seasonal effects are representative of elastic deformation, reflecting little to no residual consolidation; subsidence during the dry season is recovered during the rainy season (e.g. Hoffmann, Zebker, Galloway, & Amelung, 2001). In contrast, the absence or small amplitude of seasonal variations (smaller than the long-term subsidence) indicates that subsidence is due to inelastic consolidation of thick aquitards. Thus, subsidence in Mexico likely result from the on-going inelastic consolidation of aquitard due to widespread aquifer depletion (Scott et al., 2010), while seasonal variations in the western United States result from elastic deformation in relation to the enforcement of water pumping regulations that limit aquifer depletion (e.g. Hoffmann et al., 2001).

6. Conclusion

Using a regional InSAR-SB time-series survey, we detected a large number of subsiding locations in central Mexico; many more than previously documented. We also identified areas with high velocity gradients resulting in a great potential for fault-or fracture system formation. These observations have major implications for local hazard assessment as well as land use and city planning. We confirmed that the primary cause of land subsidence is the intense groundwater extraction of aquifer–aquitard systems for agricultural, urban, and in a few instances industrial purposes leading to a decrease in water access and quality and a non-sustainable groundwater management situation in the long term.

In many locations we found that high velocity gradients limit the subsiding areas and coincide with pre-existing faults, the apparent reactivation of these older faults being driven by the subsidence process and the groundwater recharge/extraction balance. The strong differential motions across these faults suggest that they partition the aquifer systems. The integration of InSAR with traditional monitoring techniques and flow modeling is necessary to implement effective groundwater management schemes and sustainable use of resources at regional scales.

Acknowledgments

EC thanks the National Aeronautics and Space Administration (NASA) for support NESSF 11-Earth11F-0229. FA thanks NASA for support NNX09AK72G and the National Science Foundation (NSF) for support EAR 0810214. SW thanks NASA for the research grant NNX12AQ08G. ECC was supported through grants from UNAM_PAPIIT IN121515, IN114907, IN117909, IN108611-2, and IN104213-2, and CONACYT projects 61212, 82868, and CB-101515. The ALOS-PALSAR data are copyright of the Japanese Space Agency (JAXA) and the Japanese Ministry of Economy, Trade and Industry (METI) and were made available by the U.S. Government Research Consortium (USGRC) and the Alaska Satellite Facility (ASF).

Appendix A. Supplementary data

Supplementary data associated with this article can be found in the online version, at http://dx.doi.org/10.1016/j.rse.2013.08.038. These data include Google maps of the most important areas described in this article.

References

Alaniz-Álvarez, S. A., & Nieto-Samaniego, A. F. (2007). Geology of México: Celebrating the centenary of the Geological Society of México. *Geological Society of America Special Papers, 422*.

Alba, F. (1982). *The population of Mexico: Trends, issues, and policies*. New Brunswick, NJ: Transaction.

Amelung, F., Galloway, D. L., Bell, J., Zebker, H. A., & Laczniak, R. (1999). Sensing the ups and downs of Las Vegas: InSAR reveals structural control of land subsidence and aquifer-system deformation. *Geology, 27*(6), 483–486.

Avila-Olivera, J. A., Farina, P., Garduño-Monroy, V. H., Oleschko, K., Cherkasov, S., Prieto, J. L. P., et al. (2008). Integration of InSAR and GIS in the study of surface faults caused by subsidence–creep–fault processes in Celaya, Guanajuato, Mexico (vol. 1009, pp. 200–211). *Presented at the GIS In Geology and Earth Sciences: 4th International Conference "In Vista of New Approaches for the Geoinformatics," AIP*, http://dx.doi.org/10.1063/1.2937287.

Bawden, G. W., Thatcher, W., Stein, R. S., Hudnut, K. W., & Peltzer, G. (2001). Tectonic contraction across Los Angeles after removal of groundwater pumping effects. *Nature, 412*(6849), 812–815.

Bell, J., Amelung, F., Ferretti, A., Bianchi, M., & Novali, F. (2008). Permanent Scatterer InSAR reveals seasonal and long-term aquifer-system response to groundwater pumping and artificial recharge. *Water Resources Research, 44*(2), W02,407.

Berardino, P., Fornaro, G., Lanari, R., & Sansosti, E. (2002). A new algorithm for surface deformation monitoring based on small baseline differential SAR

interferograms. *IEEE Transactions on Geoscience and Remote Sensing*, *40*(11), 2375–2383, http://dx.doi.org/10.1109/TGRS.2002.803792.

Bock, Y., Wdowinski, S., Ferretti, A., Novali, F., & Fumagalli, A. (2012). Recent subsidence of the Venice Lagoon from continuous GPS and interferometric synthetic aperture radar. *Geochemistry, Geophysics, Geosystems*, *13*, Q03023, http://dx.doi.org/10.1029/2011GC003976.

Borgia, A., Tizzani, P., Solaro, G., Manzo, M., Casu, F., Luongo, G., et al. (2005). Volcanic spreading of Vesuvius, a new paradigm for interpreting its volcanic activity. *Geophysical Research Letters*, *32*(3), L03303, http://dx.doi.org/10.1029/2004GL022155.

Bürgmann, R., Hilley, G., Ferretti, A., & Novali, F. (2006). Resolving vertical tectonics in the San Francisco bay area from Permanent Scatterer InSAR and GPS analysis. *Geology*, *34*(3), 221.

Cabral-Cano, E., Arciniega-Ceballos, A., Diaz-Molina, O., Cigna, F., Ávila-Olivera, A., Osmanoglu, B., et al. (2010b). *Is there a tectonic component to the subsidence process in Morelia, Mexico?* : IAHS-AISH Publication, 164–169.

Cabral-Cano, E., Diaz-Molina, O., & Delgado Granados, H. (2011). Subsidencia y sus mapas de peligro: Un ejemplo en el área nororiental de la Zona Metropolitana de la Ciudad de México. *Boletín de la Sociedad Geológica Mexicana*, *63*(1), 53–60.

Cabral-Cano, E., Dixon, T. H., Miralles-Wilhelm, F., Diaz-Molina, O., Sanchez-Zamora, O., & Carande, R. E. (2008). Space geodetic imaging of rapid land subsidence in Mexico City. *Geological Society of America Bulletin*, *120*(11–12), 1556–1566, http://dx.doi.org/10.1130/B26001.1.

Cabral-Cano, E., Osmanoglu, B., Dixon, T. H., Wdowinski, S., Demets, C., Cigna, F., et al. (2010a). *Subsidence and fault hazard maps using PSI and permanent GPS networks in central Mexico.* : IAHS-AISH Publication, 255–259.

Cabral-Cano, E., Solano-Rojas, D., Hernández-Espriu, A., Cigna, F., Wdowinski, S., Osmanoglu, B., et al. (2012). Subsidence induced faulting hazard risk maps in Mexico City and Morelia, central Mexico. *EOS Trans. AGU, Fall Meet. Suppl.* (Abstract 1494986).

Caine, J. S., Evans, J. P., & Forster, C. B. (1996). Fault zone architecture and permeability structure. *Geology*, *24*(11), 1025–1028, http://dx.doi.org/10.1130/0091-7613(1996)024<1025:FZAAPS>2.3.CO;2.

Calderhead, A. I., Martel, A., Alasset, P. J., Rivera, A., & Garfias, J. (2010). Land subsidence induced by groundwater pumping, monitored by D-InSAR and field data in the Toluca Valley, Mexico. *Canadian Journal of Remote Sensing*, *36*(1), 9–23.

Calderhead, A. I., Therrien, R., Rivera, A., Martel, R., & Garfias, J. (2011). Simulating pumping-induced regional land subsidence with the use of InSAR and field data in the Toluca Valley, Mexico. *Advances in Water Resources*, *34*(1), 83–97, http://dx.doi.org/10.1016/j.advwatres.2010.09.017.

Carreón-Freyre, D., Cerca, M., & Hernández Marín, M. (2005b). Propagation of fracturing related to land subsidence in the Valley of Queretaro, Mexico. *Proc. 7th Int. Symp. on Land Subsidence, 1.* (pp. 155–164).

Carreón-Freyre, D., Cerca, M., Luna-González, L., & Gámez-González, F. J. (2005a). Influencia de la estratigrafía y estructura geológica en el flujo de agua subterránea del Valle de Querétaro. *Revista Mexicana de Ciencias Geológicas*, *22*(1), 1–18.

Castillo, R. R., & Aguirre, A. S. (2010). Structural control on the subsidence faults alignment in Irapuato-Mexico. *AQUAmundi*, *01007*, 045–049, http://dx.doi.org/10.4409/Am-009-10-0007.

Casu, F., Manzo, M., & Lanari, R. (2006). A quantitative assessment of the SBAS algorithm performance for surface deformation retrieval from DInSAR data. *Remote Sensing of Environment*, *102*(3–4), 195–210, http://dx.doi.org/10.1016/j.rse.2006.01.023.

Center for International Earth Science Information Network (CIESIN), Columbia University, & Centro Internacional de Agricultura Tropical (CIAT) (2005). *Gridded Population of the World, version 3 (GPWv3): Population density grid.* Palisades, NY: NASA Socioeconomic Data and Applications Center (SEDAC) http://sedac.ciesin.columbia.edu/data/set/gpw-v3-population-density. December 2012

Chaussard, E., & Amelung, F. (2012). Precursory inflation of shallow magma reservoirs at west Sunda volcanoes detected by InSAR. *Geophysical Research Letters*, *39*(21), L21311, http://dx.doi.org/10.1029/2012GL053817.

Chaussard, E., Amelung, F., Abidin, H., & Hong, S. -H. (2013a). Sinking cities in Indonesia: ALOS PALSAR detects rapid subsidence due to groundwater and gas extraction. *Remote Sensing of Environment*, *128*, 150–161, http://dx.doi.org/10.1016/j.rse.2012.10.015.

Chaussard, E., Amelung, F., & Aoki, Y. (2013b). Characterization of open and closed volcanic systems in Indonesia and Mexico using InSAR time-series. *Journal of Geophysical Research-Solid Earth*, http://dx.doi.org/10.1002/jgrb.50288.

Cigna, F., Cabral-Cano, E., Osmanoglu, B., Dixon, T. H., & Wdowinski, S. (2011). Detecting subsidence-induced faulting in Mexican urban areas by means of persistent scatterer interferometry and subsidence horizontal gradient mapping. *Igarss*, 1–4.

Cigna, F., Osmanoglu, B., Cabral-Cano, E., Dixon, T. H., Ávila-Olivera, J. A., Garduño-Monroy, V. H., et al. (2012). Monitoring land subsidence and its induced geological hazard with Synthetic Aperture Radar Interferometry: A case study in Morelia, Mexico. *Remote Sensing of Environment*, *117*(C), 146–161, http://dx.doi.org/10.1016/j.rse.2011.09.005.

CNA (2004). *Estadísticas del agua en México.* SGAA México: Comisión Nacional del Agua. Gerencia del Registro Publico del Agua (78 pp.).

Colesanti, C., Ferretti, A., Novali, F., Prati, C., & Rocca, F. (2003). SAR monitoring of progressive and seasonal ground deformation using the permanent scatterers technique. *IEEE Transactions on Geoscience and Remote Sensing*, *41*(7), 1685–1701.

Dixon, T. H., Amelung, F., Ferretti, A., Novali, F., Rocca, F., Dokka, R., et al. (2006). Space geodesy: Subsidence and flooding in New Orleans. *Nature*, *441*(7093), 587–588, http://dx.doi.org/10.1038/441587a.

Farina, P., Avila-Olivera, J. A., & Garduño-Monroy, V. H. (2007). Structurally-controlled urban subsidence along the Mexican Volcanic Belt (MVB) monitored by InSAR. *Proc. "Envisat Symposium 2007", Montreux, Switzerland 23–27 April 2007.*

Farina, P., Avila-Olivera, J. A., Garduño-Monroy, V. H., & Catani, F. (2008). DInSAR analysis of differential land subsidence affecting urban areas along the Mexican Volcanic Belt (MVB). *Rivista Italiana Di Telerilevamento (AIT), Il Telerilevamento a Microonde, L'attività Di Ricerca E Le Applicazioni*, *40*(2), 103–113.

Fattahi, H., & Amelung, F. (2013). DEM error correction in InSAR time-series. *IEEE Transactions on Geoscience and Remote Sensing*, http://dx.doi.org/10.1109/TGRS.2012.2227761.

Ferretti, A., Fumagalli, A., Novali, F., Prati, C., Rocca, F., & Rucci, A. (2011). A new algorithm for processing interferometric data-stacks: SqueeSAR. *IEEE Transactions on Geoscience and Remote Sensing*, *49*(9), 3460–3470, http://dx.doi.org/10.1109/TGRS.2011.2124465.

Gabriel, A., Goldstein, R., & Zebker, H. A. (1989). Mapping small elevation changes over large areas — Differential radar interferometry. *Journal of Geophysical Research-Solid Earth and Planets*, *94*, 9183–9191.

Galloway, D. L., & Burbey, T. J. (2011). Review: Regional land subsidence accompanying groundwater extraction. *Hydrogeology Journal*, *19*(8), 1459–1486, http://dx.doi.org/10.1007/s10040-011-0775-5.

García-Palomo, A., Macías, J., & Garduno, V. (2000). Miocene to recent structural evolution of the Nevado de Toluca volcano region, Central Mexico. *Tectonophysics*, *318*, 281–302.

Gayol, R. (1925). Estudio de las perturbaciones que en el fondo de la Ciudad de México ha producido el drenaje de las aguas del subsuelo, por las obras del desague y rectificación de los errores a que ha dado lugar una incorrecta interpretación de los efectos producidos. *Revista Mexicana de Ingeniería y Arquitectura, III*, 96–132.

Gourmelen, N., Amelung, F., Casu, F., Manzo, M., & Lanari, R. (2007). Mining-related ground deformation in Crescent Valley, Nevada: Implications for sparse GPS networks. *Geophysical Research Letters*, *34*(9), http://dx.doi.org/10.1029/2007GL029427.

Gourmelen, N., Amelung, F., & Lanari, R. (2010). Interferometric synthetic aperture radar–GPS integration: Interseismic strain accumulation across the Hunter Mountain fault in the eastern California shear zone. *Journal of Geophysical Research*, *115*(B9), B09408, http://dx.doi.org/10.1029/2009JB007064.

Helm, D. C. (1978). Field verification of a one-dimensional mathematical model for transient compaction and expansion of a confined aquifer system. *Verification of mathematical and physical models in hydraulic engineering* (pp. 189–196)Proceedings 26th Hydraulic Division Specialty Conference.

Hiriart, F., & Marsal, R. J. (1969). The subsidence of Mexico City. *Volumen nabor carrillo, comision impulsora y coordinadora de la investigacion cientifica, 47.* (pp. 109–147) Mexico City: Sec. de Hacienda y Credito Publico.

Hoffmann, J., Zebker, H. A., Galloway, D. L., & Amelung, F. (2001). Seasonal subsidence and rebound in Las Vegas Valley, Nevada, observed by synthetic aperture radar interferometry. *Water Resources Research*, *37*(6), 1551–1566.

Hooper, A. (2006). *Persistent scatter radar interferometry for crustal deformation studies and modeling of volcanic deformation.* (Ph.D. thesis). : Stanford University.

Huizar-Álvarez, R., Mitre-Salazar, L. M., Marín-Córdova, S., Trujillo-Candelaria, J., & Martínez-Reyes, J. (2011). Subsidence in Celaya, Guanajuato, Central Mexico: Implications for groundwater extraction and the neotectonic regime. *Geofisica Internacional*, *50*(3), 255–270.

INEGI (2011). *Censo Nacional de Poblacion, 2010, Mexico.* : Instituto Nacional de Estadistica, Geografia e Informatica.

Julio-Miranda, P., Ortíz-Rodríguez, A. J., Palacio-Aponte, A. G., López-Doncel, R., & Barboza-Gudiño, R. (2012). Damage assessment associated with land subsidence in the San Luis Potosi–Soledad de Graciano Sanchez metropolitan area, Mexico, elements for risk management. *Natural Hazards*, *64*(1), 751–765, http://dx.doi.org/10.1007/s11069-012-0269-3.

Kampes, B. (2005). *Displacement parameter estimation using permanent scatterer interferometry.* (Ph.D. thesis). : Technische Universiteit Delft.

Kampes, B. (2006). *Radar interferometry — Persistent scatterer technique, remote sensing and digital image processing, 12,* : Springer.

Lanari, R., Casu, F., Manzo, M., Zeni, G., Berardino, P., Manunta, M., et al. (2007). An overview of the small baseline subset algorithm: A DInSAR technique for surface deformation analysis. *Pure and Applied Geophysics*, *164*(4), 637–661.

Lanari, R., Mora, O., Manunta, M., Mallorquí, J. J., Berardino, P., & Sansosti, E. (2004). A small-baseline approach for investigating deformations on full-resolution differential SAR interferograms. *IEEE Transactions on Geoscience and Remote Sensing*, *42*(7), 1377–1386.

Leake, S. A. (1990). Interbed storage changes and compaction in models of regional groundwater flow. *Water Resources Research*, *26*(9), 1939–1950.

López-Quiroz, P., Doin, M. -P., Tupin, F., Briole, P., & Nicolas, J. M. (2009). Time-series analysis of Mexico City subsidence constrained by radar interferometry. *Journal of Applied Geophysics*, *69*(1), 1–15, http://dx.doi.org/10.1016/j.jappgeo.2009.02.006.

Maclay, R. W., & Small, T. A. (1983). Hydrostratigraphic subdivisions and fault barriers of the Edwards aquifer, south-central Texas, USA. *Journal of Hydrology*, *61*(1), 127–146.

Massonnet, D., Rossi, M., Carmona, C., Adragna, F., Peltzer, G., Feigl, K. L., et al. (1993). The displacement field of the Landers earthquake mapped by radar interferometry. *Nature*, *364*, 138–142.

Mazari, M., & Alberro, J. (1991). *Hundimiento de la Ciudad de México.* Los Problemas de la Cuenca de México: Mexico City, Mexico, El Colegio Nacional, 83–114.

Mazzotti, S., Lambert, A., Van der Kooij, M., & Mainville, A. (2009). Impact of anthropogenic subsidence on relative sea-level rise in the Fraser River delta. *Geology*, *37*(9), 771–774, http://dx.doi.org/10.1130/G25640A.1.

Meckel, T. A., Brink, ten, U. S., & Williams, S. J. (2006). Current subsidence rates due to compaction of Holocene sediments in southern Louisiana. *Geophysical Research Letters*, *33*(11), http://dx.doi.org/10.1029/2006GL026300.

Nieto-Samaniego, A. F., Alaniz-Álvarez, S. A., & Camprubí, A. (2007). Mesa Central of México: Stratigraphy, structure, and Cenozoic tectonic evolution (vol. 422, pp. 41–70). *Geological Society of America*, http://dx.doi.org/10.1130/2007.2422(02).

Ortega-Guerrero, A., Rudolph, D. L., & Cherry, J. A. (1999). Analysis of long-term land subsidence near Mexico City: Field investigations and predictive modeling. *Water Resources Research*, *35*(11), 3327–3341.

Ortiz-Zamora, D., & Ortega-Guerrero, A. (2010). Evolution of long-term land subsidence near Mexico City: Review, field investigations, and predictive simulations. *Water Resources Research*, *46*(1), W01513, http://dx.doi.org/10.1029/2008WR007398.

Osmanoglu, B., Dixon, T. H., Wdowinski, S., Cabral-Cano, E., & Jiang, Y. (2011). Mexico City subsidence observed with persistent scatterer InSAR. *International Journal of Applied Earth Observations and Geoinformation*, *13*(1), 1–12, http://dx.doi.org/10.1016/j.jag.2010.05.009.

Pacheco, J., Arzate, J., Rojas, E., Arroyo, M., Yutsis, V., & Ochoa, G. (2006). Delimitation of ground failure zones due to land subsidence using gravity data and finite element modeling in the Querétaro valley, México. *Engineering Geology*, *84*(3–4), 143–160, http://dx.doi.org/10.1016/j.enggeo.2005.12.003.

Poland, J. F. (1961). The coefficient of storage in a region of major subsidence caused by compaction of an aquifer system. *U.S. Geological Survey Professional Paper*, *424-B*, 52–54.

Rodríguez, R., Lira, J., & Rodríguez, I. (2012). Subsidence risk due to groundwater extraction in urban areas using fractal analysis of satellite images. *Geofisica Internacional*, *51*(2), 157–167.

Rosen, P. A., Hensley, S., Peltzer, G., & Simons, M. (2004). Updated repeat orbit interferometry package released. *Eos, Transactions of the American Geophysical Union*, *85*(5), 47, http://dx.doi.org/10.1029/2004EO050004.

Sánchez-Mejorada, R. (2000). Mining law in Mexico. *Mineral Resources Engineering*, *9*(1), 129–139.

Schmidt, D. A., & Bürgmann, R. (2003). Time-dependent land uplift and subsidence in the Santa Clara valley, California, from a large interferometric synthetic aperture radar data set. *Journal of Geophysical Research*, *108*(B9), 2416, http://dx.doi.org/10.1029/2002JB002267.

Schroeder, A., & Rodríguez, R. (2010). Subsidence faulting and aquifer vulnerability — their relation in Irapuato, Mexico. *IAHS Publications-Series of Proceedings and Reports-Intern Assoc Hydrological Sciences*, *339*. (pp. 502–504).

Scott, C. A., Dall'erba, S., & Caravantes, R. D. (2010). Groundwater rights in Mexican agriculture: Spatial distribution and demographic determinants. *The Professional Geographer*, *62*(1), 1–15, http://dx.doi.org/10.1080/00330120903375837.

Servicio Geologico Mexicano (1998). Edición de cartas geológico-mineras y geoquímicas escala 1:250,000. http://www.sgm.gob.mx/cartas/Cartas_Ed.jsp.

Sestini, G. (1996). Land subsidence and sea-level rise: The case of the Po Delta region, Italy. In J.D. Milliman, & B. U. Haq (Eds.), *Sea-level rise and coastal subsidence* (pp. 235–248). : Kluwer Academic Publishers.

Singh, S., & Pardo, M. (1993). Geometry of the Benioff zone and state of stress in the overriding plate in central Mexico. *Geophysical Research Letters*, *20*(14), 1483–1486.

Strozzi, T., & Wegmuller, U. (1999). Land subsidence in Mexico City mapped by ERS differential SAR interferometry. *Geoscience and Remote Sensing Symposium, IGARSS '99 Proceedings. IEEE 1999 International*, *4*. (pp. 1940–1942).

Strozzi, T., Wegmuller, U., Werner, C. L., Wiesmann, A., & Spreckels, V. (2003). JERS SAR interferometry for land subsidence monitoring. *IEEE Transactions on Geoscience and Remote Sensing*, *41*(7), 1702–1708, http://dx.doi.org/10.1109/TGRS.2003.813273.

Strozzi, T., Werner, C. L., Wegmuller, U., & Wiesmann, A. (2005). Monitoring land subsidence in Mexico City with Envisat ASAR Interferometry. *Proc. of the 2004 Envisat & ERS Symposium, Salzburg, Austria 6-10 September 2004*, *572*. (pp. 154).

Teatini, P., Tosi, L., & Strozzi, T. (2011). Quantitative evidence that compaction of Holocene sediments drives the present land subsidence of the Po Delta, Italy. *Journal of Geophysical Research*, *116*(B8), B08407, http://dx.doi.org/10.1029/2010JB008122.

Terzaghi, K. (1925). *Erdbaumechanik (introduction to soil mechanics)*. Vienna: Franz Deuticke, 1943–1944.

Teufel, L. W. (1987). Permeability changes during shear deformation of fractured rock. *Proceedings of the 28th U. S. Symposium on Rock Mechanics*, *28*. (pp. 473–480).

Tizzani, P., Berardino, P., Casu, F., Euillades, P., Manzo, M., Ricciardi, G. P., et al. (2007). Surface deformation of Long Valley Caldera and Mono Basin, California, investigated with the SBAS–InSAR approach. *Remote Sensing of Environment*, *108*(3), 277–289, http://dx.doi.org/10.1016/j.rse.2006.11.015.

Usai, S. (2003). A least squares database approach for SAR interferometric data. *IEEE Transactions on Geoscience and Remote Sensing*, *41*(4), 753–760, http://dx.doi.org/10.1109/TGRS.2003.810675.

Valera, J. L., & Stange, A. J. (2011). New oil contracts not likely to help Mexico's declining oil production. *Oil and Gas Financial Journal* (http://www.ogfj.com/articles/2011/01/new-oil-contracts-not-likely-to-help-mexico-s.html)

Vega, F. G. E. (1976). Subsidence of the city of Mexico: a historical review, Proceedings of the Second International Symposium on land Subidence, Anaheim, International Association of Hydrological Science. *UNESCO publication No.*, *121*, 35–38.

Wright, T. J., Parsons, B. E., & Lu, Z. (2004). Toward mapping surface deformation in three dimensions using InSAR. *Geophysical Research Letters*, *31*(1), L01607, http://dx.doi.org/10.1029/2003GL018827.

Yan, Y., Doin, M. -P., López-Quiroz, P., Tupin, F., Fruneau, B., Pinel, V., et al. (2012). Mexico City subsidence measured by InSAR time-series: Joint analysis using PS and SBAS approaches. *IEEE Journal of Selected Topics in Applied Earth Observations and Remote Sensing*, *5*(4), 1312–1326, http://dx.doi.org/10.1109/JSTARS.2012.2191146.

Yan, X. X., & Gong, S. L. (2002). Relationship between building density and land subsidence in Shanghai urban zone (in Chinese). *Hydrogeology and Engineering Geology*, *29*(6), 21–25.